



# A multi-physics process model for simulating the manufacture of resin-infused composite aerostructures



Robert S. Pierce<sup>a, b, \*</sup>, Brian G. Falzon<sup>b</sup>, Mark C. Thompson<sup>a</sup>

<sup>a</sup> Department of Mechanical and Aerospace Engineering, Monash University, Melbourne, VIC 3800, Australia

<sup>b</sup> School of Mechanical and Aerospace Engineering, Queen's University Belfast, BT9 5AH, United Kingdom

## ARTICLE INFO

### Article history:

Received 3 April 2017

Received in revised form

29 June 2017

Accepted 2 July 2017

Available online 3 July 2017

### Keywords:

Fabrics/textiles

Deformation

Modelling

Resin infusion

## ABSTRACT

The increasing demand for large, complex and low-cost composite aerostructures has motivated advances in the simulation of liquid composite moulding techniques with textile reinforcement materials. This work outlines the development and validation of a multi-physics process model that better simulates infusion behaviour through a complex preform compared with traditional models used in industry that do not account for fabric deformation. By combining the results of a preform draping model with deformation-dependent permeability properties, the shape and local flow characteristics of a deformed textile reinforcement have been more realistically defined for infusion. Simulated shear deformation results were used to define the distributed permeability properties across the fabric domain of the infusion model. Full-scale vacuum infusion experiments were conducted for a complex double dome geometry using a plain weave carbon fibre material. The multi-physics process model showed significant improvement over basic models, since it is able to account for the change in flow behaviour that results from local fabric deformation.

© 2017 Elsevier Ltd. All rights reserved.

## 1. Introduction

The commercial aircraft industry continually strives to manufacture lighter, larger and more complex structures at a reduced cost and timescale. Composite materials have the potential to offer significant benefits in terms of light-weighting and part-count reduction, as components can be manufactured with greater complexity and integration than with traditional metallic structures. A further desire to reduce manufacturing costs and time cycles is also prompting a transition from traditional autoclave manufacturing techniques to liquid composite moulding methods using textile reinforcement materials. In a typical liquid composite moulding process, a dry reinforcement material is first formed to the desired part geometry. Then liquid resin is introduced to infuse the preform, before a curing process produces the final composite component. This tends to be less expensive than autoclave manufacturing, however these methods often rely on operator skill and experience through empirical practices. Consequently, in the production of new, large and complex composite structures there

can be considerable losses resulting from wasted time, labour and material investment.

Process modelling aims to replace empirical practices with a realistic simulation of the manufacturing process. Such modelling efforts have the potential to anticipate the occurrence of production defects, subsequently reducing production timescales and overall costs. For liquid composite moulding techniques with fabric reinforcement materials, there are three integral aspects to the generation of a full multi-physics simulation: material characterisation, drape modelling and infusion modelling. Additionally, it is important to ensure that such a simulation can account for the effect of fabric deformation on the permeability and subsequent infusion behaviour.

### 1.1. Material characterisation

During draping, it is the shear response of a fabric that primarily dictates the deformation behaviour [1], with the high tensile modulus of fibres providing a secondary contribution. Bending stiffness is also known to influence the nature of out-of-plane wrinkling behaviour [2], though it is commonly neglected in simulations where the accurate topology of the wrinkles is not required [3,4]. Hence, the tensile, shear and even bending properties of a

\* Corresponding author. School of Mechanical and Aerospace Engineering, Queen's University Belfast, BT9 5AH, United Kingdom.

E-mail address: [r.pierce@qub.ac.uk](mailto:r.pierce@qub.ac.uk) (R.S. Pierce).

woven reinforcement material are often characterised to improve the accuracy of the draping model.

Although there have been studies on the biaxial nature of fabric tensile behaviour [5], there remains no standard method for the biaxial tensile testing of fabric materials. Subsequently, it is more common to use a uniaxial approach, such as the ASTM strip test [6].

The shear characterisation of textile materials also remains unstandardised despite the well-known significance of fabric shear behaviour on draping [7]. Currently, there are two approaches in popular use: the picture frame test [8] and the bias extension method [9,10]. These tests have been evaluated and compared in the literature [11], revealing the picture frame test to have clamp-tension and alignment issues, while the bias extension test is unreliable for direct kinematic measurements [12]. Recent research has also investigated the coupling between tensile and shear properties in order to better understand preform behaviour and wrinkling [9]. However, this work is more relevant for processes that impart considerable tension on the preform material during deformation, such as stamping.

Regarding the infusion of resin through a porous preform material, Darcy's law in Equation (1), can be used to relate volume-averaged flow velocity,  $\mathbf{v}$ , with resin viscosity,  $\mu$ , material permeability,  $\mathbf{K}$ , and the driving pressure gradient,  $\nabla P$ .

$$\mathbf{v} = -\frac{\mathbf{K}}{\mu} \cdot \nabla P \quad (1)$$

For the purposes of modelling, the unknown flow velocity requires knowledge of these material and fluid properties, among which the pressure gradient and resin viscosity are relatively simple to measure and control. Hence, accurate permeability characterisation is particularly important in support of modelling efforts.

Despite significant research [13–15], there remains no standardised method for textile permeability characterisation. Coordinated benchmarking efforts have shown that there can be a great degree of variability in permeability testing, where similar experiments have produced results that vary by a whole order of magnitude [13]. Other research has investigated predictive modelling for the characterisation of permeability properties, however such work still relies on experimental validation [16].

In woven reinforcement materials, two-dimensional flow is known to exhibit an elliptical shape. Hence, Weitzenböck et al. [17] demonstrated that anisotropic permeability properties could be characterised by two principal permeability values,  $K_1$  and  $K_2$ , and a principal permeability direction,  $\phi$ . Additionally, since fabric deformation changes the internal architecture of a fabric weave, permeability properties also need to be characterised in relation to the shear deformation. This effect has been investigated both experimentally [18,19] and with predictive modelling [19–21].

## 1.2. Drape modelling

Draping models aim to predict fabric deformation behaviour during the manufacture of complex structural components. Primarily, these can determine the final part shape, however knowledge of the internal deformation behaviour is also valuable. Some models use discrete methods to simulate fibre behaviour within the fabric yarns [22], although semi-discrete [23] or continuum approaches [3,4] are more commonly used to approximate the internal deformation behaviour. Fabric shear behaviour, facilitated by yarn reorientation, is well known to be the primary deformation mode for textile materials [1]. Hence accurate yarn tracking becomes particularly important for the determination of shear strain (shear angle).

## 1.3. Infusion modelling

Resin infusion modelling typically aims to predict the resin flow behaviour and fill time for manufacturing processes. The most popular methods tend to be variations of the Control Volume/Finite Element (CVFE) approach and the Volume of Fluid (VOF) method. Both methods have seen some success, and are capable of simulating merging flows and variable preform thickness [24]. However, VOF methods can be advantageous for resolving adjacent regions with significantly different permeability characteristics [25]. Notable studies using finite element based models have also investigated specific issues related to void formation [24,26], bag compaction [27] and distribution media collapse [28]. In practice though, most industrial modelling applications rely on isotropic and/or homogenous permeability properties throughout the infusion domain, regardless of the geometric or material complexity [25,29]. This is often reasonable for flat laminates, but not for complex structures, since preform deformation is known to have a significant effect on local permeability properties [19,30].

## 1.4. Combined process model

As the draping and infusion behaviour are related, the need to combine them in a single process model is well documented [30–32]. Previous efforts to develop such a multi-physics process model have seen some success [30], also with a focus on saturation effects [33,34]. However, such models have not seen full-scale experimental validation. Hence, this paper demonstrates the development and validation of a new multi-physics process model that accounts for deformation-dependent flow behaviour, compared against full-scale experiments.

## 2. Process model design

The new multi-physics process model relies on the integration of various simulation and testing elements shown in Fig. 1. A draping model is first used to predict the fabric deformation during forming and an infusion model is then employed to simulate the

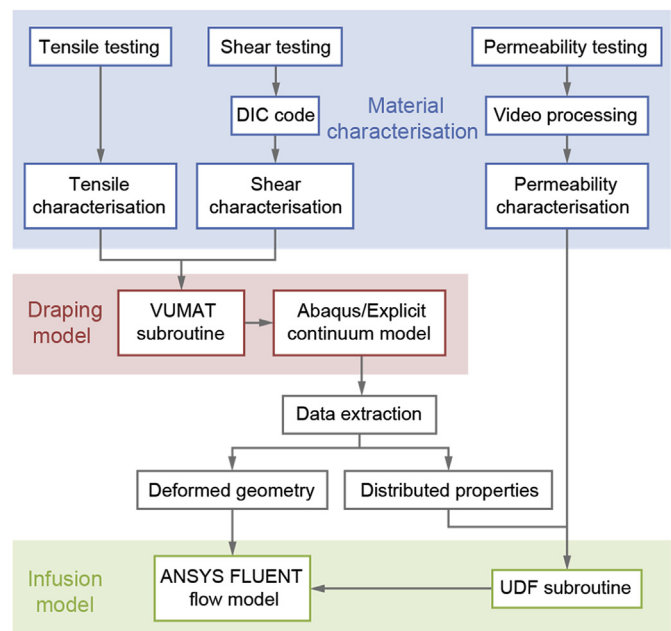


Fig. 1. Flow diagram of the multi-physics process model.

flow of resin through the deformed reinforcement material. However, the accuracy of these models also depends upon comprehensive material characterisation.

Dry tensile and shear fabric properties support the mechanical material model, while deformation-dependent permeability properties feed into the infusion model and facilitate the link between the two simulation stages. A digital image correlation (DIC) code is used to accurately characterise shear deformation during material testing and an explicit user-defined (VUMAT) subroutine then describes this fabric behaviour within Abaqus. Additionally, a user defined function (UDF) subroutine for ANSYS FLUENT is used to assign variable deformation-dependent permeability properties across the material domain.

In the following sections of this paper, the individual elements of the process model are addressed in greater detail, before a final validation of the working model is demonstrated.

### 3. Material characterisation

Characterisation of the preform behaviour was essential to the accuracy of subsequent modelling efforts. These characterisation experiments included mechanical tensile and shear testing, along with permeability testing, for an aerospace grade carbon fibre fabric. A dry, and relatively loose, plain weave fabric was used as the preform material, with 3 K tows and an areal density of 0.193 kg/m<sup>2</sup>.

#### 3.1. Tensile characterisation

A uniaxial strip test method (ASTM D5035-11) [6] was employed to characterise the fabric tensile behaviour. Five samples were prepared according to the standard, for both the warp and weft fibre directions. Tests were conducted on an Instron 4505 frame with updated 5500R electronics, using a 5 kN load cell, under a 0.5 mm/min cross-head displacement rate. The tensile ‘strain’ was measured from the overall fabric response, including de-crimping effects, since the true strain within the fibre tows is more difficult to measure and implement within the draping modelling. ‘Stress’ was calculated by assuming a constant and homogenous cross-section, since the resulting properties were intended for a continuum draping model with the same cross-section and homogeneity assumption.

Ultimately, these tests were found to be highly repeatable for both yarn directions, with a negligible difference in the warp and weft strain results. Subsequently, a fourth order polynomial was generated in Equation (2) to best fit the experimental elastic

modulus as a function of tensile strain. Fig. 2 shows the corresponding stress-strain curves for the experimental data, including the curve resulting from the polynomial fit of the elastic modulus. Here the polynomial fit clearly captures both the initial de-crimping behaviour of the woven fabric and the high tensile stiffness response of the carbon fibre tows.

$$E = \left( -8.951 \times 10^8 \epsilon^4 + 3.458 \times 10^6 \epsilon^3 - 5.525 \times 10^5 \epsilon^2 + 4.18 \times 10^3 \epsilon + 3.8 \right) \text{ GPa} \tag{2}$$

#### 3.2. Shear characterisation

For this research, the bias extension test was used for shear characterisation due to its relative simplicity. This also helped to avoid the known clamping and alignment issues with picture frame testing [12]. However, since direct mechanical shear measurement in bias extension testing is often unreliable [12], an optical strain measurement technique had to be used instead.

Samples were cut with a gauge region of 100 mm × 50 mm, oriented such that the long testing direction bisected the warp and weft yarn directions. This meant that samples were extended in what is known as the fabric ‘bias’ direction. Such a test produces several different regions of shear deformation, shown in Fig. 3: a diamond-shaped central shear zone that undergoes ‘pure’ shearing, two triangular regions next to the clamps that exhibit no shearing and four half-sheared triangular regions. Tests were run under a displacement rate of 10 mm/min on an Instron 5948 MicroTester machine with a 0.1 kN load cell, which provided considerable accuracy at lower loads.

A digital camera was used to record images of each sample at regular intervals. MATLAB code was developed to perform Digital

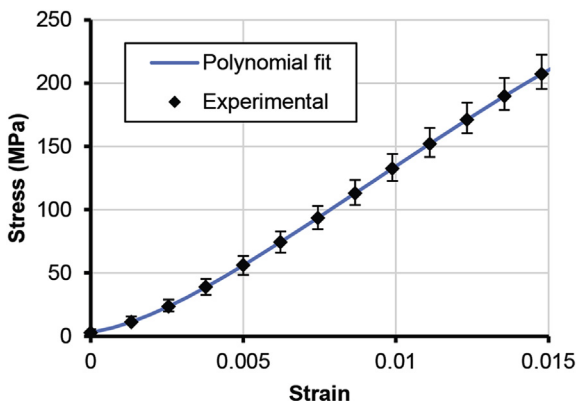


Fig. 2. Polynomial curve of Young’s modulus versus strain (error bars represent the maximum and minimum measured values).

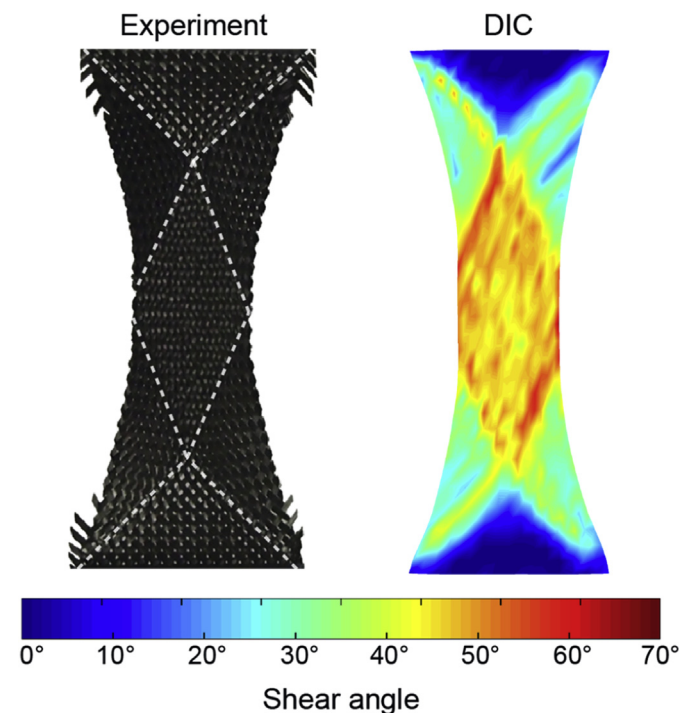


Fig. 3. Experimental bias extension and Digital Image Correlation (DIC) results at 20 mm extension.

Image Correlation (DIC) and calculate the strain behaviour throughout each sample [35]. This code essentially correlates point-based features from across the samples through a sequence of images in order to determine a distribution of nodal displacements. From these displacements, the deformation gradient can be calculated for groups of adjacent nodes and the 'true' fibre directions can be calculated in order to find a detailed shear angle (shear strain) distribution across the whole sample (as shown in Fig. 3). Full details of the theory behind these calculations can be found in literature [35].

Shear angles from the central shear zone were then averaged in order to calculate the shear modulus based on a theoretical normalised shear force, outlined by Lebrun et al. [11]. An exponential function was found to provide the best fit for the shear response, as shown in Equation (3). A simple polynomial curve fit was not sufficient to capture this behaviour, although similar approximations have been used in previous studies [3,36]. Fig. 4 shows the stress-strain behaviour from this curve fit against experimental results, which captures both the relative freedom of fibre tow rotation at low shear angles (shear strain) and the significant stiffening behaviour that occurs during shear locking.

$$G_{12} = \left( 0.008196e^{4.24\gamma} + 1.056 \times 10^{-11}e^{23.69\gamma} \right) \text{ MPa} \quad (3)$$

### 3.3. Permeability characterisation

Permeability characterisation was necessary in order to support the infusion model and to quantify the influence of shear fabric deformation. An unsaturated radial flow experiment was employed in this work, as it allowed for two-dimensional permeability characterisation where the principal permeability directions were unknown prior to testing. Although permeability testing is more commonly performed on thicker stacks of material plies to reduce wall effects [13], a single-ply configuration (300 mm × 300 mm) was selected to eliminate the influence of nesting. This also provided the best demonstration of the relationship between deformation and infusion behaviour. Fig. 5 shows the experimental configuration of the permeability tests conducted under a vacuum-driven constant injection pressure, where fabric samples were sandwiched between parallel glass and polycarbonate plates. White breather was placed cloth around the sample periphery to ensure an even pressure gradient throughout the samples and the test cavity was measured to be 0.4 mm using a laser displacement sensor. Given the relative thinness of these plates, it was important to ensure that any potential effect resulting from cavity deflection

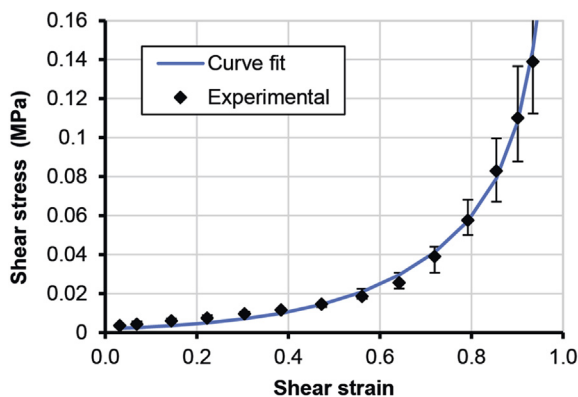


Fig. 4. Exponential curve of shear modulus function against shear strain (error bars represent the maximum and minimum measured values).

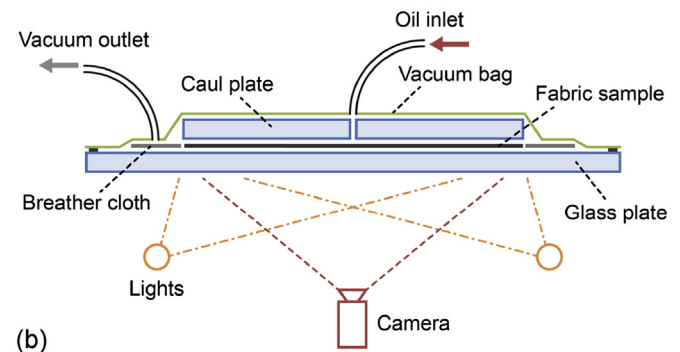
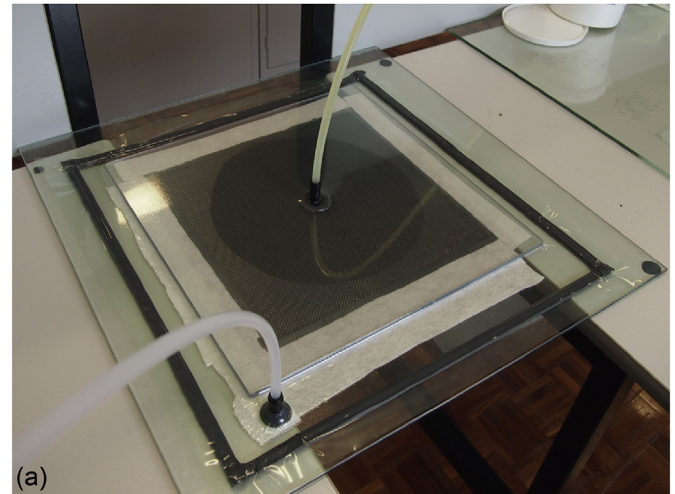


Fig. 5. Radial permeability test: (a) an un-sheared sample, (b) full configuration schematic.

was negligible via both regression analysis [37] and flow simulations through a constant thickness domain as described in Section 5.2. Through-thickness and gravitational effects were neglected due to the thinness of the single ply samples, and a 3 mm radius inlet was used to introduce oil into the samples.

The woven carbon fibre material was tested for a range of fabric shear angles (0°–40°), in batches of at least six samples. Olive oil was used as the test fluid, since its standard room temperature viscosity (0.084 Pa s) was consistent with the viscosity of typical infusion resins (between 0.001 Pa s and 0.3 Pa s) [38]. Complete details of the experimental method can be found in previous work [37].

An in-house MATLAB code was developed to process video footage of the experimental flow front propagation and calculate directional permeability. This code used a statistical approach to define principal permeability values,  $K_1$  and  $K_2$ , and the principal permeability direction,  $\phi$ , with greater confidence [37].

From these experiments, a detailed profile for deformation-dependent permeability behaviour was determined according to Equations (4) and (5) (see also Fig. 6). The principal permeability direction,  $\phi$ , was initially found to coincide with the bias direction, bisecting the warp and weft yarns. The local porosity,  $\phi$ , was simply defined according to the original undeformed porosity,  $\phi_0$ , and fabric shear angle,  $\gamma$ , as shown in Equation (6).

$$K_1 = \left( -6.641\gamma^4 + 13.28\gamma^3 - 8.414\gamma^2 + 2.4\gamma + 0.6028 \right) \times 10^{-10} \text{ m}^2 \quad (4)$$

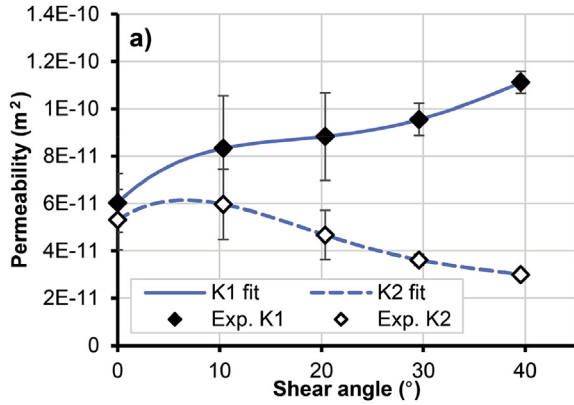


Fig. 6. Principal permeability properties relative to fabric shear angle (error bars represent the standard deviation).

$$K_2 = \left( -7.7\gamma^4 + 14.66\gamma^3 - 9.261\gamma^2 + 1.605\gamma + 0.5313 \right) \times 10^{-10} \text{ m}^2 \quad (5)$$

$$\phi = 1 - \frac{1 - \phi_0}{\cos \gamma} \quad (6)$$

As the fabric shear angles increased,  $K_1$  values increased,  $K_2$  values decreased (after a slight initial increase) and subsequently the anisotropy greatly increased. However, in order to use this data for the demonstration of the process model, further calibration was required. The original permeability experiments were performed with fabric samples sandwiched between two rigid plates to ensure that cavity deflection would not influence the results. Alternatively, the process model demonstration was to be performed between a rigid mould and a deformable vacuum bag. Hence, several additional tests were run without the rigid caul plate, directly under a vacuum bag, to determine the effect of the bag and a suitable calibration estimate. In these tests, bridging of the vacuum bag between tows served to reduce overall flow through the fabric. Additionally, considerable anisotropy was also observed at shear angles below  $20^\circ$ , which was not present in the original permeability experiments. As a result of this calibration exercise the deformation-dependent permeability properties,  $K_1$  and  $K_2$ , for the model demonstration trials were reduced by a constant 33% and 50% of the original values from Equations (4) and (5) respectively. To further account for the bagged anisotropy, the principal permeability direction,  $\phi$ , was adjusted with a bias towards the weft yarn direction at low shear angles, according to Equation (7).

$$\phi = \begin{cases} \frac{|\gamma|}{20^\circ} \left( 45^\circ - \frac{|\gamma|}{2} \right) & \text{if } |\gamma| \leq 20^\circ \\ 45^\circ - \frac{|\gamma|}{2} & \text{if } |\gamma| > 20^\circ \end{cases} \quad (7)$$

The permeability calibration served as a correction for the bagging process, which could not be measured from the permeability characterisation experiments. The calibration percentages remained constant for the full range of deformation and were consistent across all modelling efforts regardless of fabric orientation. Subsequently, the relative flow behaviour through different regions of deformation and for different forming trials remains comparable. However this bagging effect will need to be studied further in future research.

#### 4. Draping model

The draping model for this research is based on a continuum hypoelastic approach within Abaqus/Explicit, following the success of Khan et al. [3] and Peng et al. [4]. With this method, fabric layers are represented as continuous sheets of M3D4R membrane (or S4R shell) elements, and a VUMAT material subroutine is used to replicate the internal deformation behaviour. This approach neglects yarn slippage and bending but still allows for simulations with thicker, multiple-ply preforms. The VUMAT subroutine was developed to track the non-orthogonal change in yarn orientations during deformation and calculate the fabric response from the experimental material characteristics,  $E$  and  $G_{12}$ , presented in Equations (2) and (3) respectively. Full details of the theory and implementation of this subroutine can also be found in previous literature [39].

#### 5. Resin infusion model

The capability to simulate the transient behaviour of two interacting fluid phases (resin and air), and local changes in anisotropic permeability, are essential to the success of the multi-physics process model. Since this work focuses on the significance of deformation-dependent permeability behaviour; isothermal conditions are assumed, while saturation and compaction effects are largely neglected. However, future consideration of these factors is not outside the capability of the presented infusion modelling approach. Based on overall flexibility, reliability and availability, ANSYS FLUENT was found to be the most appropriate Computational Fluid Dynamics (CFD) package for this infusion modelling work.

##### 5.1. Theory

Fundamentally, the infusion model is based on a Eulerian Volume of Fluid (VOF) approach, similar to that first proposed by Hirt and Nichols [40]. Resin and air phases are treated as interpenetrating continua where the volume of one phase cannot be occupied by any other phase. The volume fractions of the two phases are traced through the domain cells and are used to calculate cell-averaged properties within a common flow field. Therefore, only one set of governing equations needs to be solved for the two phases [41].

This multiphase modelling approach employs the following governing equations. Firstly, the momentum equation (8), which neglects inter-phase mass transfer but includes gravitational acceleration,  $\mathbf{g}$ , and source terms,  $\mathbf{S}_K$ .

$$\frac{\partial}{\partial t}(\rho \mathbf{u}) + \nabla \cdot (\rho \mathbf{u} \otimes \mathbf{u}) = -\nabla p + \nabla \cdot \left[ \mu (\nabla \mathbf{u} + \nabla \mathbf{u}^T) \right] + \rho \mathbf{g} + \mathbf{S}_K \quad (8)$$

The momentum source term,  $\mathbf{S}_K$ , is used to introduce the permeability characteristics,  $K$ , of the porous media as a loss defined by Equation (9).

$$\mathbf{S}_K = -\frac{\mu}{K} \mathbf{u} \quad (9)$$

To account for the multiple fluid phases, the momentum equation is essentially a single-phase transport equation with variable viscosity and density depending on the volume fraction of each phase in a cell. These variable density,  $\rho$ , and viscosity,  $\mu$ , parameters are described by Equation (10), simply as averages of the fractional content of each phase in a cell.

$$\rho = V_{fp}\rho_{resin} + (1 - V_{fp})\rho_{air}, \quad \mu = V_{fp}\mu_{resin} + (1 - V_{fp})\mu_{air} \quad (10)$$

Next, the continuity and volume fraction equation (11), also neglects mass transfer between phases and any additional source terms.

$$\frac{\partial}{\partial t}(V_{fp,\alpha}\rho_\alpha) + \nabla \cdot (V_{fp,\alpha}\rho_\alpha \mathbf{u}) = 0 \quad (11)$$

Here,  $V_{fp,\alpha}$  is the resin volume fraction of phase  $\alpha$ , and the volume fractions of all phases sum to unity according to Equation (12).

$$\sum_{\alpha=1}^{N_p} V_{fp,\alpha} = 1 \quad (12)$$

Before being passed on to the solver, Equation (11) is divided by phasic density and summed over all the fluid phases in Equation (13), where  $N_p$  is the number of phases.

$$\sum_{\alpha=1}^{N_p} \frac{1}{\rho_\alpha} \left( \frac{\partial}{\partial t}(V_{fp,\alpha}\rho_\alpha) + \nabla \cdot (V_{fp,\alpha}\rho_\alpha \mathbf{u}) \right) = 0 \quad (13)$$

It is also possible to include an energy equation within the VOF method to account for non-adiabatic processes, although for this work such considerations are neglected. Ultimately, the governing equations are solved iteratively due to the non-linear and coupled behaviour, using a pressure-based solver algorithm.

## 5.2. Validation

The validity of this infusion model was evaluated against the anisotropic experimental permeability test results. This ensured that the VOF method was accurately simulating anisotropic fluid flow through a porous material and allowed for an investigation of any mesh or time-step dependence.

Radial flow experiments from the characterisation of permeability properties were simulated using the FLUENT infusion model. Undeformed ( $0^\circ$ ) and sheared ( $40^\circ$ ) domains were set up with 300 mm edge lengths and 0.4 mm thickness. The modelling parameters for both cases were consistent with experimental conditions and are outlined in Table 1.

The simulated flow front results in Fig. 7 are representative of all modelling cases, showing good agreement with the experimental flow. Since the VOF approach in FLUENT produces a relatively diffuse flow front, the contour line of 0.5 oil/air volume fraction was considered as the discrete flow front for direct comparison against the experimental results. Plotting such flow front progression for both  $0^\circ$  and  $40^\circ$  sheared cases in Fig. 7, the simulations show a

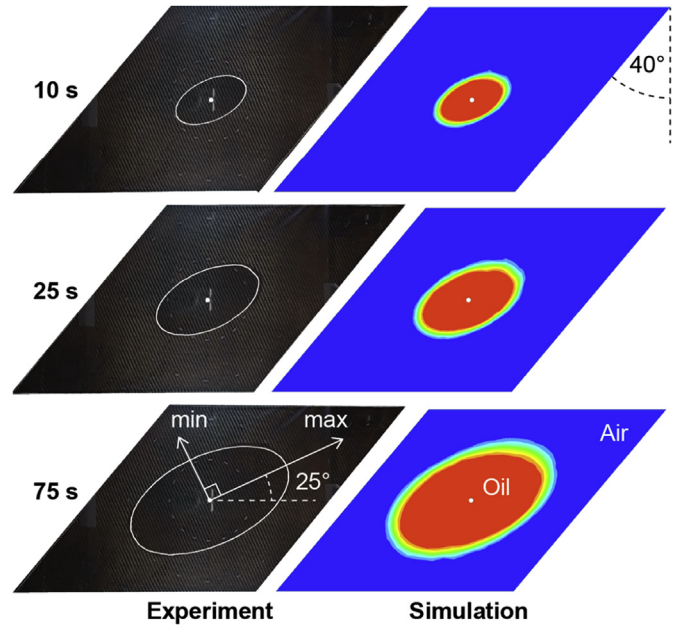


Fig. 7. Comparison of experimental and simulated flow front progression in  $40^\circ$  sheared samples.

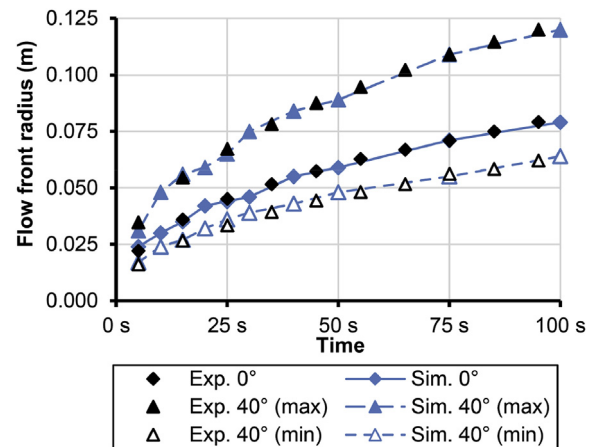


Fig. 8. Flow front progression in simulated and experimental permeability tests for  $0^\circ$  and  $40^\circ$  sheared samples.

Table 1

Parameters for simulating oil flow in both isotropic and anisotropic permeability characterisation experiments.

Fabric shear angle	$0^\circ$ (isotropic)	$40^\circ$ (anisotropic)
Pressure differential (kPa)	98	98.5
Fluid viscosity (Pa.s)	0.0882	0.0805
Fluid density ( $\text{kg}/\text{m}^3$ )	850	
Air viscosity (Pa.s)	1.983e-5	
Air density ( $\text{kg}/\text{m}^3$ )	1.225	
Porosity	0.724	0.640
Permeability, $K_1$ ( $\text{m}^2$ )	5.7e-11	11.1e-11
Permeability, $K_2$ ( $\text{m}^2$ )	–	3.0e-11
Principal permeability direction, $\varphi$ (relative to weft yarn direction)	–	$25^\circ$

mean error of less than 2% from the experimental results. These results also confirm the validity of the permeability experiments, as the simulated constant cavity thickness shows very good agreement with each test under similar conditions (see Fig. 8).

## 6. Process model integration

In order to more realistically simulate liquid composite moulding compared with traditional methods, the individual components of the process model have all been combined, according to Fig. 1. Traditional models commonly assume that fabric properties are homogenous [29]; even in cases where various pre-determined zones are assigned different permeability properties, due to flow enhancing media or changing preform thickness, each zone itself remains homogenous. This is reasonable for cases where the formed geometry is very simple, like in flat panels. However for complex structures one must account for the effect of fabric deformation on flow behaviour. This concept of modelling resin

infusion based on the true deformed state of the reinforcement material has been theorised for some years. Hence, this research creates a novel link between accurate draping model results and the generation of distributed permeability properties in a subsequent infusion model.

Due to incompatibilities between Abaqus and FLUENT, the two models are connected in two stages. First, the Abaqus draping results are extracted from a binary output database (odb) file and exported to intermediate files using a Python script related to the Abaus Scripting Interface. Second, the data from these files is imported into the infusion model for processing and analysis.

### 6.1. Extracting the draping results

The Python script devoted to exporting draping results operates by first identifying the location of the object file and the contained data relating to the final state of the simulation. Then the node labels, element labels and indices for the deformable material body are stored. Assuming the deformable material body is rectangular, this also serves as an opportunity to determine the grid size in terms of rows and columns. Subsequently, the deformed nodal coordinates, integration point coordinates, local material direction vectors and shear angle values for each element are also stored before being written to two output text files.

The new 'deformed geometry' file contains all the nodal position data such that remodelling of the draped part can be easily performed in the ANSYS software suite. Hence, the stored grid of 3D deformed node coordinates are grouped by column and listed row-by-row. The other 'distributed properties' file contains the element number, coordinates of the integration point, local material direction vectors and shear angles associated with each listed element.

### 6.2. Importing data into the infusion model

To set up the infusion model, the 'deformed geometry' data is first used to recreate an appropriate flow domain in the ANSYS DesignModeller package. This process of model regeneration requires only three steps with minimal user interaction. The nodal position data from the 'deformed geometry' file is formatted such that it can be imported as a series of '3D curves' to form the skeleton of the model. Then the 'skin/loft' feature within the software can be used to create the full 3D domain based on the skeletal curves. Lastly this domain needs to be meshed before it can be used for the infusion model.

Upon initialisation of the infusion model, a User Defined Function (UDF) subroutine reads the 'distributed properties' and stores them. In case the mesh of the infusion model is not identical to that of the draping model, this subroutine interpolates the centroid properties of each cell using an inverse distance-based weighting method for the nearest three draping mesh neighbours. The alignment of the local permeability tensor in each cell is defined by Equation (7), the shear angle and the local material direction vectors from the draping model. Cell permeability properties are defined by the shear angle and calibrated versions of Equations (4) and (5).

Because the permeability properties and orientations are expected to remain constant throughout the infusion simulation, these calculations are only performed once upon model initialisation. This helps to minimise computational effort. Values associated with each cell location are then stored such that they can be quickly recalled as necessary throughout the flow simulation.

## 7. Process model validation

Vacuum infusion experiments were performed over a large

'double dome' tool in order to validate simulation results from the complete process model. This geometry is commonly used in literature to evaluate the performance of draping models, due to its complex double curvature [3,4]. Hence it was a natural selection for this investigation.

### 7.1. Experimental set-up

A male double dome tool was constructed from structural foam, coated, and recessed 120 mm into an outer frame (950 mm × 550 mm), such that the top of the male tool was flush with the top of the outer frame (as seen in Fig. 9). This improved the material forming and bag conformity, since simply bagging the male tool caused bag wrinkling and race-tracking during infusion.

Single plies of the dry, plain weave carbon fibre fabric were cut to 800 mm × 500 mm in various orientations. These were marked with a 50 mm silver grid to facilitate optical measurements during both forming and infusion. Tests for the 90°/0° and -45°/45° warp/weft yarn orientations are presented as the focus of this paper. A deformable vacuum bag was then placed over the mould. This was chosen in preference over a rigid mould for several reasons. Firstly, a transparent upper mould was necessary to observe the flow front. Such a large and complex, clear rigid mould would be not only challenging to manufacture with suitable tolerances but also to implement and use. The vacuum bag, on the other hand, could maintain good conformity under ambient pressure and was more consistent with the intended industrial application. Distribution media was placed under the inlet and outlet ports to enhance flow in these critical areas.

During the forming process, the central port was first connected to the vacuum pump to initiate the bag and preform deformation. As the bag reached the bottom of the mould, the secondary vacuum ports at the ends of the mould were instead connected to the vacuum pump and the central port was closed-off. The preform material and vacuum bag were then checked for conformity to ensure that no bridging was occurring in the concave regions of the mould.

Next, for the infusion process, the central vacuum port was connected to an open oil reservoir to act as the fluid inlet. As with the permeability characterisation experiments, olive oil was selected as the experimental fluid since it has a relatively low

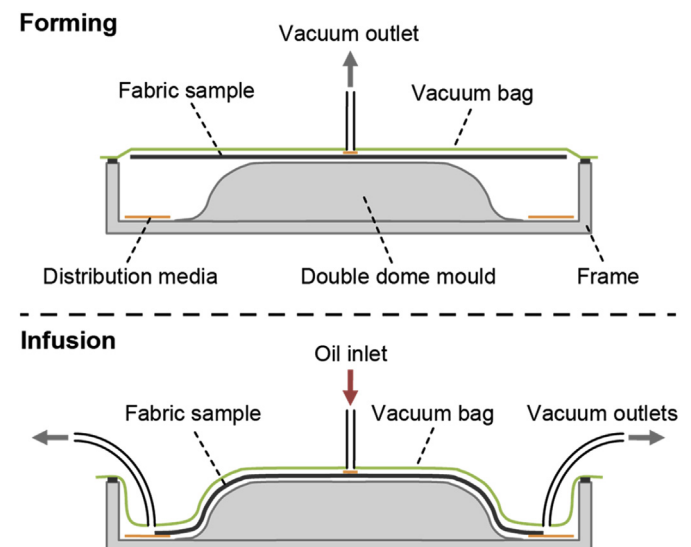


Fig. 9. Two-stage process for the double dome demonstration experiments.

viscosity that is representative of infusion resins [38]. Fig. 9 shows the forming and infusion stages of the demonstration experiments. During infusion the experimental flow front was monitored with regular digital images for comparison against the flow predictions.

### 7.2. Numerical modelling

For simplicity, the Abaqus draping model was set up with a stamping configuration rather than replicating the vacuum forming approach exactly. The fabric was held in place between a rigid blank holder and die, and then a rigid male punch formed the material into its final shape. This approach was very similar to previous double dome forming simulations from literature [3,4]. The simulated fabric blank was 0.4 mm thick and modelled in quarter- and half-symmetry for the  $90^\circ/0^\circ$  and  $-45^\circ/45^\circ$  cases respectively.

The non-linear tensile and shear properties from Equations (2) and (3) were included in the VUMAT subroutine for the draping model. A global contact condition for tangential friction (0.15) was applied across the entire model, based on results from a parametric study in accordance with general practices [3,4,36]. Each fabric ply was meshed with 1000–2000 M3D4R membrane elements, depending on the degree of symmetry. The punch, binder and die parts were represented as analytical rigid bodies with finer R3D3 element meshes. Results from the draping model were then extracted using the automated Python script to produce the deformed geometry and distributed properties files for compatibility with the ANSYS infusion model.

The infusion modelling stage required regeneration of the double dome geometry in the ANSYS software suite, before a 50 mm diameter central inlet was partitioned from the material domain to represent the distribution media inlet conditions. Due to the symmetry of the models, a single outlet condition was applied to one end of the material domain. All faces other than the outlet and inlet were defined using symmetric (free-slip) wall conditions, in accordance with the same assumptions from the permeability characterisation experiments. The simulated inlet and outlet pressures were set to 101.3 kPa and 0.3 kPa respectively, and the undeformed baseline porosity for the plain weave material was 0.724. As a result of different experimental temperature conditions, oil viscosities for the  $90^\circ/0^\circ$  and  $-45^\circ/45^\circ$  orientation cases were 0.0756 Pa s and 0.0993 Pa s respectively.

The porosity, principal permeability values ( $K_1$  and  $K_2$ ) and directions ( $\varphi$ ) were all defined on a cell-by-cell basis by the UDF subroutine in relation to the shear angle distribution from draping, local material directions and the calibrated experimental permeability functions.

Mesh convergence and time-step dependence were investigated to determine the optimal balance of solution time and accuracy. Subsequent flow front predictions for a 1000–2000 element mesh and 1 s time-step exhibited less than 2% variance from the mesh and time-step independent results. Fig. 10 shows the fluid inlet and vacuum outlet definitions for the quarter-symmetry  $90^\circ/0^\circ$  orientation domain. This image also depicts the distribution of  $K_2$  principal permeability vectors that were assigned throughout the domain. In this case, the  $K_2$  principal permeability direction was initially aligned with the warp yarn direction in areas with minimal shear deformation, but rotated towards the fabric bias direction (bisecting the warp and weft yarn directions) as the shear angle increased, according to Equation (6).

### 7.3. Draping results

During draping the vacuum bag and fabric material were seen to conform well to the double dome mould (as seen in Fig. 11), for all cases, without any wrinkling. There was also good symmetry in all

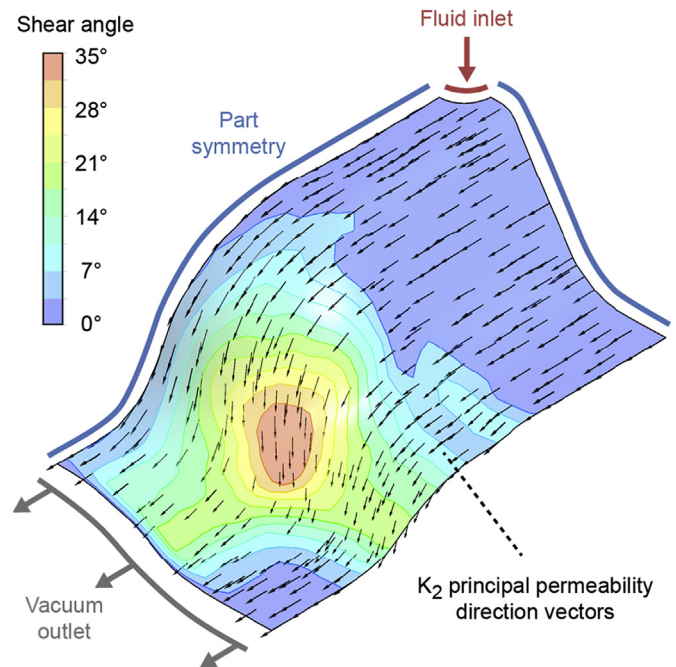


Fig. 10. Example of the  $90^\circ/0^\circ$  infusion modelling case within FLUENT.

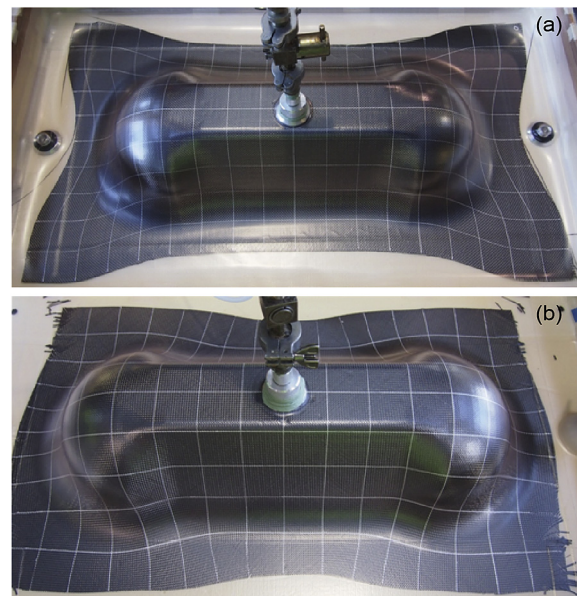


Fig. 11. Formed double dome samples for: (a)  $90^\circ/0^\circ$  and, (b)  $-45^\circ/45^\circ$  cases.

forming trials with only minor yarn fraying at the material edges.

In order to compare the form of the draped fabric against the results of the draping model, mean experimental position values were calculated as an average of eight similar experimental grid locations. Subsequently, the modelled points were found to have less than 2% error from the mean experimental results for all orientations.

The fidelity of the draping simulation was further evaluated by comparing the predicted shear angle values against experimental shear angle results. Examples of values for 16 locations in the  $90^\circ/0^\circ$  and  $-45^\circ/45^\circ$  cases are shown in Figs. 12 and 13 respectively. The experimental values reflect the mean results from all symmetrical

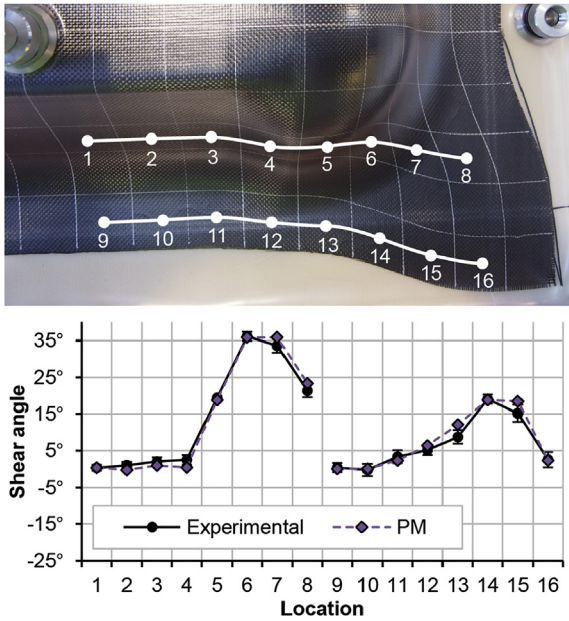


Fig. 12. Comparison of experimental and simulated (PM) shear angles for the 90°/0° case.

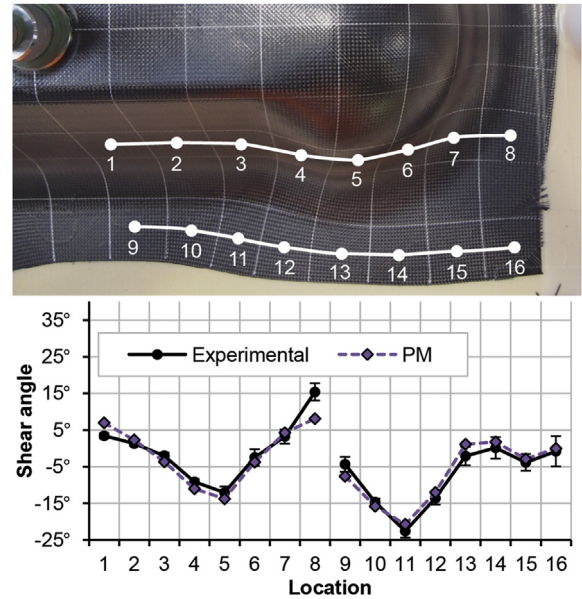


Fig. 13. Comparison of experimental and simulated (PM) shear angles for the -45°/45° case.

quadrants of repeated tests, with error bars depicting the standard deviation. Overall, the predicted shear angle values showed very good agreement with the experimental results at all locations.

7.4. Infusion results

In order to assess the success of the process model during infusion, the simulated flow front progression over time has been compared to both experimental results and a ‘basic’ infusion model. This ‘basic’ model simply assumes that the fabric permeability properties are isotropic and deformation-independent, based on the mean unsheared permeability properties after calibration ( $K_1 = K_2 = 3.3 \times 10^{-11} m^2$ ). Figs. 14 and 15 highlight the flow front position for both models and experiments, in each case. Again, the simulated flow front corresponds to the contour line for 0.5 vol fraction of oil and air.

It can be seen that the flow behaviour is well captured by the model, since regions of high shear deformation correspond with increased permeability and faster flow, as was observed experimentally. Similarly, the anisotropy is also well captured by the process model, particularly in the -45°/45° case where flow in the weft direction is more pronounced than that in the warp direction. It is important to note that the photographed flow fronts, highlighted in Figs. 14 and 15, include some perspective distortion introduced by the wide-angle camera lens. However, for more accurate quantitative results, basic geometric calculations were employed to account for this photographic distortion, since the exact tool geometry and deformed grid dimensions were known. Figs. 16 and 17 show the more accurate flow front advancement, accounting for image distortion, for the process model and experimental tests in both cases. These results show some remaining variance in the modelled and experimental results. Compaction is expected to be a major contributor to this variance, since the model does not account for changes in bag compaction that may result from changing fluid pressure. Additionally, unstandardised permeability characterisation and calibration is expected to have had a considerable effect on these results. However, the general flow behaviour is well captured despite these limitations,

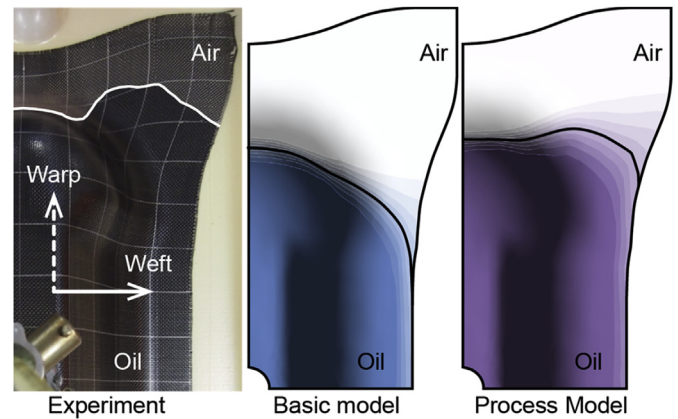


Fig. 14. Flow front comparison at 1255 s for the 90°/0° case.

particularly when compared against existing basic models.

7.5. Multiple plies

The single-ply simulations have provided a good demonstration of the model’s capabilities against a more basic model that does not account for deformation-dependent infusion behaviour. However, a single-ply case is of limited value in industrial applications. Hence it is important to note that while multiple ply experiments have not been conducted for this work, the process model is not limited to single-ply applications. The Abaqus draping model, FLUENT infusion model and supporting subroutines are all capable of multiple ply considerations. For example, each ply can be modelled with its own continuum domain, accounting for inter-ply interactions such as friction and fluid transfer. Hence, future work aims to demonstrate the validity of this approach for more realistic applications.

8. Conclusion

A multi-physics computational approach is presented for

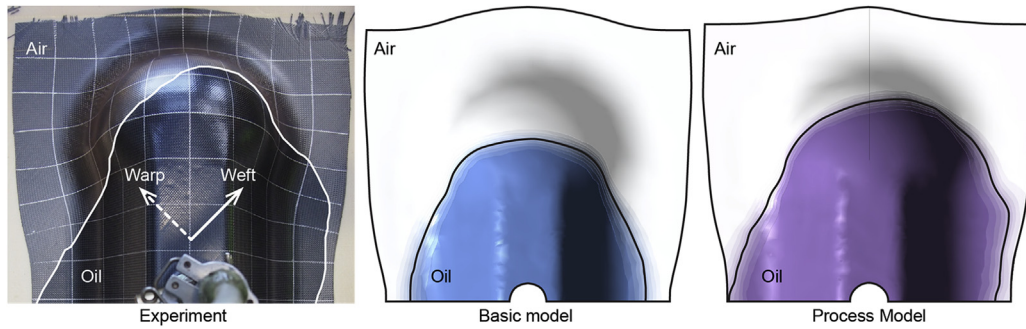


Fig. 15. Flow front comparison at 850 s for the  $-45^\circ/45^\circ$  case.

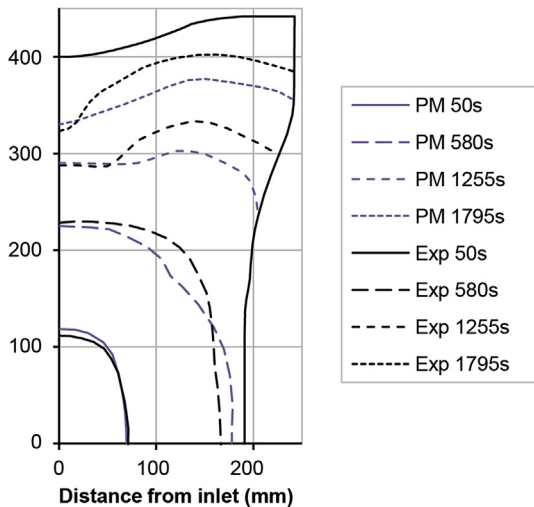


Fig. 16. Experimental and simulated (PM) transient flow front results for the  $90^\circ/0^\circ$  case.

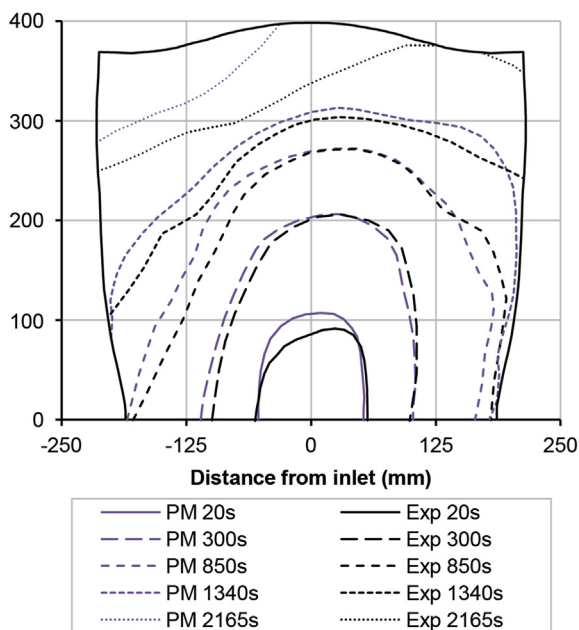


Fig. 17. Experimental and simulated (PM) transient flow front results for the  $-45^\circ/45^\circ$  case.

simulating liquid composite moulding processes with textile reinforcement materials. Aerospace grade carbon fibre fabric samples have been experimentally characterised to determine tensile, shear and permeability properties. These properties have been incorporated into a continuum-based finite element draping model and a volume of fluid infusion model for improved realism. The results of the draping model have been linked to the infusion model, such that the characterised relationship between shear deformation and fabric permeability can be used to predict the complex distribution of permeability properties throughout a preform prior to infusion.

The process model has been validated against vacuum infusion experiments for a complex double dome demonstrator part. The draping component of the process model predicts material draw-in and shear deformation (shear angles) with good accuracy. Furthermore, using realistic permeability properties, the infusion simulations demonstrate a significant improvement in the prediction of flow front behaviour over traditional models. Overall, the novel multi-physics process model shows good agreement with validation experiments, particularly in areas of high shear deformation, which significantly affect local flow behaviour.

## Acknowledgements

This research was supported under the Australian Research Council's 'Linkage Projects' funding scheme (LP100100508) in partnership with Boeing Research & Technology Australia. The second author would also like to acknowledge the financial support of Bombardier and the Royal Academy of Engineering.

## References

- [1] B. Zhu, T.X. Yu, X.M. Tao, Large deformation and slippage mechanism of plain woven composite in bias extension, *Compos. Part A Appl. Sci. Manuf.* 38 (2007) 1821–1828, <http://dx.doi.org/10.1016/j.compositesa.2007.04.009>.
- [2] P. Boisse, N. Hamila, E. Vidal-Sallé, F. Dumont, Simulation of wrinkling during textile composite reinforcement forming. Influence of tensile, in-plane shear and bending stiffnesses, *Compos. Sci. Technol.* 71 (2011) 683–692, <http://dx.doi.org/10.1016/j.compscitech.2011.01.011>.
- [3] M.A. Khan, T. Mabrouki, E. Vidal-Sallé, P. Boisse, Numerical and experimental analyses of woven composite reinforcement forming using a hypoelastic behaviour. Application to the double dome benchmark, *J. Mater. Process. Technol.* 210 (2010) 378–388, <http://dx.doi.org/10.1016/j.jmatprotec.2009.09.027>.
- [4] X. Peng, Z.U. Rehman, Textile composite double dome stamping simulation using a non-orthogonal constitutive model, *Compos. Sci. Technol.* 71 (2011) 1075–1081, <http://dx.doi.org/10.1016/j.compscitech.2011.03.010>.
- [5] P. Boisse, A. Gasser, G. Hivet, Analyses of fabric tensile behaviour: determination of the biaxial tension-strain surfaces and their use in forming simulations, *Compos. Part A Appl. Sci. Manuf.* 32 (2001) 1395–1414, [http://dx.doi.org/10.1016/S1359-835X\(01\)00039-2](http://dx.doi.org/10.1016/S1359-835X(01)00039-2).
- [6] ASTM International, ASTM D5035–11, Standard Test Method for Breaking Force and Elongation of Textile Fabrics (Strip Method), West Conshohocken, PA, 2011, <http://dx.doi.org/10.1520/D5035-11>.
- [7] J. Cao, R. Akkerman, P. Boisse, J. Chen, H.S. Cheng, E.F. De Graaf, J.L. Gorczyca, P. Harrison, G. Hivet, J. Launay, W. Lee, L. Liu, S.V. Lomov, A. Long, E. De

- Luycker, F. Morestin, J. Padvoiskis, X.Q. Peng, J. Sherwood, T. Stoilova, X.M. Tao, I. Verpoest, A. Willems, J. Wiggers, T.X. Yu, B. Zhu, Characterization of mechanical behavior of woven fabrics: experimental methods and benchmark results, *Compos. Part A Appl. Sci. Manuf.* 39 (2008) 1037–1053, <http://dx.doi.org/10.1016/j.compositesa.2008.02.016>.
- [8] M.F. Culpin, The shearing of fabrics: a novel approach, *J. Text. Inst.* 70 (1979) 81–88, <http://dx.doi.org/10.1080/00405007908631522>.
- [9] P. Harrison, F. Abdiwi, Z. Guo, P. Potluri, W.R. Yu, Characterising the shear-tension coupling and wrinkling behaviour of woven engineering fabrics, *Compos. Part A Appl. Sci. Manuf.* 43 (2012) 903–914, <http://dx.doi.org/10.1016/j.compositesa.2012.01.024>.
- [10] P. Potluri, D.A. Perez Ciurezu, R.B. Ramgulum, Measurement of meso-scale shear deformations for modelling textile composites, *Compos. Part A Appl. Sci. Manuf.* 37 (2006) 303–314, <http://dx.doi.org/10.1016/j.compositesa.2005.03.032>.
- [11] G. Lebrun, M.N. Bureau, J. Denault, Evaluation of bias-extension and picture-frame test methods for the measurement of intraply shear properties of PP/glass commingled fabrics, *Compos. Struct.* 61 (2003) 341–352, [http://dx.doi.org/10.1016/S0263-8223\(03\)00057-6](http://dx.doi.org/10.1016/S0263-8223(03)00057-6).
- [12] P. Harrison, M.J. Clifford, A.C. Long, Shear characterisation of viscous woven textile composites: a comparison between picture frame and bias extension experiments, *Compos. Sci. Technol.* 64 (2004) 1453–1465, <http://dx.doi.org/10.1016/j.compscitech.2003.10.015>.
- [13] R. Arbter, J.M. Beraud, C. Binetruy, L. Bizet, J. Bréard, S. Comas-Cardona, C. Demaria, A. Endruweit, P. Ermanni, F. Gommer, S. Hasanovic, P. Henrat, F. Klunker, B. Laine, S. Lavanchy, S.V. Lomov, A. Long, V. Michaud, G. Morren, E. Ruiz, H. Sol, F. Trochu, B. Verleye, M. Wietgreffe, W. Wu, G. Ziegmann, Experimental determination of the permeability of textiles: a benchmark exercise, *Compos. Part A Appl. Sci. Manuf.* 42 (2011) 1157–1168, <http://dx.doi.org/10.1016/j.compositesa.2011.04.021>.
- [14] S. Sharma, D.A. Siginer, Permeability measurement methods in porous media of fiber reinforced composites, *Appl. Mech. Rev.* 63 (2010), <http://dx.doi.org/10.1115/1.4001047>.
- [15] N. Vernet, E. Ruiz, S. Advani, J.B. Alms, M. Aubert, M. Barbuski, B. Barari, J.M. Beraud, D.C. Berg, N. Correia, M. Danzi, T. Delavière, M. Dickert, C. Di Fratta, A. Endruweit, P. Ermanni, G. Francucci, J.A. Garcia, A. George, C. Hahn, F. Klunker, S.V. Lomov, A. Long, B. Louis, J. Maldonado, R. Meier, V. Michaud, H. Perrin, K. Pillai, E. Rodriguez, F. Trochu, S. Verheyden, M. Weitgreffe, W. Xiong, S. Zaremba, G. Ziegmann, Experimental determination of the permeability of engineering textiles: benchmark II, *Compos. Part A Appl. Sci. Manuf.* 61 (2014) 172–184, <http://dx.doi.org/10.1016/j.compositesa.2014.02.010>.
- [16] C.C. Wong, A.C. Long, M. Sherburn, F. Robitaille, P. Harrison, C.D. Rudd, Comparisons of novel and efficient approaches for permeability prediction based on the fabric architecture, *Compos. Part A Appl. Sci. Manuf.* 37 (2006) 847–857, <http://dx.doi.org/10.1016/j.compositesa.2005.01.020>.
- [17] J.R. Weitzenbock, R.A. Sheno, P.A. Wilson, Measurement of three-dimensional permeability, *Compos. Part A Appl. Sci. Manuf.* (1998) 159–169, [http://dx.doi.org/10.1016/S1359-835X\(97\)00049-3](http://dx.doi.org/10.1016/S1359-835X(97)00049-3).
- [18] J. Slade, E.M. Sozer, S.G. Advani, Fluid impregnation of deformed preforms, *J. Reinf. Plast. Compos.* 19 (2000) 552–568, <http://dx.doi.org/10.1177/073168440001900703>.
- [19] A. Endruweit, P. Ermanni, The in-plane permeability of sheared textiles. Experimental observations and a predictive conversion model, *Compos. Part A Appl. Sci. Manuf.* 35 (2004) 439–451, <http://dx.doi.org/10.1016/j.compositesa.2003.11.002>.
- [20] F. Loix, P. Badel, L. Orgéas, C. Geindreau, P. Boisse, Woven fabric permeability: from textile deformation to fluid flow mesoscale simulations, *Compos. Sci. Technol.* 68 (2008) 1624–1630, <http://dx.doi.org/10.1016/j.compscitech.2008.02.027>.
- [21] C.C. Wong, A.C. Long, Modelling variation of textile fabric permeability at mesoscopic scale, *Plast. Rubber Compos.* 35 (2006) 101–111, <http://dx.doi.org/10.1179/174328906X103088>.
- [22] D. Durville, Simulation of the mechanical behaviour of woven fabrics at the scale of fibers, *Int. J. Mater. Form.* 3 (2010) 1241–1251, <http://dx.doi.org/10.1007/s12289-009-0674-7>.
- [23] S. Allaoui, P. Boisse, S. Chatel, N. Hamila, G. Hivet, D. Soulat, E. Vidal-Salle, Experimental and numerical analyses of textile reinforcement forming of a tetrahedral shape, *Compos. Part A Appl. Sci. Manuf.* 42 (2011) 612–622, <http://dx.doi.org/10.1016/j.compositesa.2011.02.001>.
- [24] E. Ruiz, V. Achim, S. Soukane, F. Trochu, J. Bréard, Optimization of injection flow rate to minimize micro/macro-voids formation in resin transfer molded composites, *Compos. Sci. Technol.* 66 (2006) 475–486, <http://dx.doi.org/10.1016/j.compscitech.2005.06.013>.
- [25] F.F. Luz, S.C. Amico, J.A. Souza, E.S. Barbosa, A.G. Barbosa de Lima, Resin transfer moulding process: fundamentals, numerical computation and experiments, in: *Numer. Anal. Heat Mass Transf. Porous Media*, first ed., Springer-Verlag Berlin Heidelberg, 2012, pp. 121–150, <http://dx.doi.org/10.1007/978-3-642-30532-0>.
- [26] C.H. Park, A. Lebel, A. Saouab, J. Bréard, W. Il Lee, Modeling and simulation of voids and saturation in liquid composite molding processes, *Compos. Part A Appl. Sci. Manuf.* 42 (2011) 658–668, <http://dx.doi.org/10.1016/j.compositesa.2011.02.005>.
- [27] Q. Govignon, S. Bickerton, P.A. Kelly, Simulation of the reinforcement compaction and resin flow during the complete resin infusion process, *Compos. Part A Appl. Sci. Manuf.* 41 (2010) 45–57, <http://dx.doi.org/10.1016/j.compositesa.2009.07.007>.
- [28] P. Šimáček, S.G. Advani, Modeling resin flow and fiber tow saturation induced by distribution media collapse in VARTM, *Compos. Sci. Technol.* 67 (2007) 2757–2769, <http://dx.doi.org/10.1016/j.compscitech.2007.02.008>.
- [29] P. Šimáček, S.G. Advani, Desirable features in mold filling simulations for liquid composite molding processes, *Polym. Compos.* 25 (2004) 355–367, <http://dx.doi.org/10.1002/pc.20029>.
- [30] B. Verleye, S.V. Lomov, A. Long, I. Verpoest, D. Roose, Permeability prediction for the meso-macro coupling in the simulation of the impregnation stage of resin transfer moulding, *Compos. Part A Appl. Sci. Manuf.* 41 (2010) 29–35, <http://dx.doi.org/10.1016/j.compositesa.2009.06.011>.
- [31] S.V. Lomov, G. Huysmans, Y. Luo, R.S. Parnas, A. Prodromou, I. Verpoest, F.R. Phelan, Textile composites: modelling strategies, *Compos. Part A Appl. Sci. Manuf.* 32 (2001) 1379–1394, [http://dx.doi.org/10.1016/S1359-835X\(01\)00038-0](http://dx.doi.org/10.1016/S1359-835X(01)00038-0).
- [32] S.G. Advani, P. Šimáček, Liquid composite molding: role of modeling and simulation in process advancement, Copenhagen, in: *20th Int. Conf. Compos. Mater.*, 2015.
- [33] J.R. Walther, *The Effect of Fabric and Fiber Tow Shear on Dual Scale Flow and Fiber Bundle Saturation during Liquid Molding of Textile Composites*, University of Delaware, 2011.
- [34] J. Walther, P. Šimáček, S.G. Advani, The effect of fabric and fiber tow shear on dual scale flow and fiber bundle saturation during liquid molding of textile composites, *Int. J. Mater. Form.* 5 (2012) 83–97, <http://dx.doi.org/10.1007/s12289-011-1060-9>.
- [35] R.S. Pierce, B.G. Falzon, M.C. Thompson, R. Boman, A low-cost digital image correlation technique for characterising the shear deformation of fabrics for draping studies, *Strain* 51 (2015) 180–189, <http://dx.doi.org/10.1111/str.12131>.
- [36] X. Peng, F. Ding, Validation of a non-orthogonal constitutive model for woven composite fabrics via hemispherical stamping simulation, *Compos. Part A Appl. Sci. Manuf.* 42 (2011) 400–407, <http://dx.doi.org/10.1016/j.compositesa.2010.12.014>.
- [37] R.S. Pierce, B.G. Falzon, M.C. Thompson, Permeability characterisation of sheared carbon fiber textile preform, *Polym. Compos.* (2016). <http://onlinelibrary.wiley.com/doi/10.1002/pc.24206/full>.
- [38] C. Williams, J. Summerscales, S. Grove, Resin infusion under flexible tooling (RIFT): a review, *Compos. Part A Appl. Sci. Manuf.* 27 (1996) 517–524, [http://dx.doi.org/10.1016/1359-835X\(96\)00008-5](http://dx.doi.org/10.1016/1359-835X(96)00008-5).
- [39] R.S. Pierce, B.G. Falzon, M.C. Thompson, R. Boman, Implementation of a non-orthogonal constitutive model for the finite element simulation of textile composite draping, *Appl. Mech. Mater.* 553 (2014) 76–81.
- [40] C.W. Hirt, B.D. Nichols, Volume of fluid (VOF) method for the dynamics of free boundaries, *J. Comput. Phys.* 39 (1981) 201–225, [http://dx.doi.org/10.1016/0021-9991\(81\)90145-5](http://dx.doi.org/10.1016/0021-9991(81)90145-5).
- [41] V.R. Gopala, B.G.M. van Wachem, Volume of fluid methods for immiscible-fluid and free-surface flows, *Chem. Eng. J.* 141 (2008) 204–221, <http://dx.doi.org/10.1016/j.cej.2007.12.035>.